

PVP2011-57278

FORCES ON PIPING BENDS DUE TO PROPAGATING DETONATIONS

Thomas C. Ligon and David J. Gross

Dominion Engineering, Inc.
Reston, Virginia, USA

Joseph E. Shepherd

Graduate Aerospace Laboratories
California Institute of Technology
Pasadena, California, USA

ABSTRACT

This paper reports the results of experiments, analytical models, and finite element simulations on the structural response of piping systems to internal detonation loading. Of particular interest are the interaction of detonations with 90° bends and the creation of forces that lead to axial and bending structural response of the piping system. The piping systems were fabricated using 304 stainless steel, 2-in. (50 mm) diameter schedule 40 commercial pipe with a nominal wall thickness of 0.154-in. (3.8 mm) and welded construction to ASME B31.3 standards. The piping was supported using custom brackets or cantilever beams fastened to steel plates that were bolted to the laboratory walls. Nearly-ideal detonations were used in a 30/70 H₂-N₂O mixture at 1 atm initial pressure and 300 K. The detonation speeds were close (within 1%) to the Chapman-Jouguet velocity and detonation cell sizes much smaller than the tube diameter. Pressure, displacement, acceleration and hoop, longitudinal, and support strains were measured using a high-speed (1 MHz) digital data acquisition system and calibrated signal conditioners.

Detonation propagation through a bend generates a longitudinal stress wave in the piping that can be observed on the strain gauges and is predicted by both analytical models and finite element simulations. The peak magnitude of the bend force is approximately twice that due to the pressure alone since the peak momentum flux of the flow behind the detonation front is comparable to the pressure in the front. With relatively simple models, quantitative predictions of the bend forces can be made for the purposes of design or safety analysis of piping systems with internal detonations.

NOMENCLATURE

A	Pipe Cross-Sectional Area
c_0	Longitudinal Sound Velocity
c_{CJ}	Sound Velocity at the CJ State

c_3	Post-Expansion Region Sound Velocity
CJ	Chapman-Jouguet
DLF	Dynamic Load Factor
E	Modulus of Elasticity
FFT	Fast Fourier Transform
γ_2	Detonation Products Ratio of Specific Heats
P_{CJ}	CJ Detonation Pressure
P_3	Post-Expansion Region Pressure
UI	Unsteady Idealized (Bend Force/Pressure Model)
ρ	Density
ν	Poisson's Ratio
QS	Quasi-Steady (Bend Force/Pressure Model)
t	Pipe Thickness
TZ	Taylor-Zel'dovich
u	Velocity
U_{CJ}	CJ Detonation Velocity
R	Pipe Mid-Radius

INTRODUCTION

The present study is motivated by safety analysis requirements of potential explosion hazards in the Hanford Tank Waste Treatment and Immobilization Plant (WTP) Project. Under some postulated accident conditions, explosive gases may build up within the piping system and ignition may result in a propagating flame that may under certain conditions [1] transition to a supersonic combustion wave known as a detonation. A detonation [2] is a dynamic load that excites a wide spectrum of mechanical vibrations in a piping system and creates an internal pressure load [3]. If a piping system is to withstand a detonation, both aspects of the loading must be considered. This means that the collective motions of all the components of the piping system must be considered through testing [4, 5] and detailed structural response computations [6]. From this point of view, the response of piping systems to

internal detonations has common elements with the evaluation of seismic and fluid transient or water hammer (see Chapters 9 and 11 of Antaki [7] and Chapters 34, 36, 37 of Rao [8]) excitation of piping systems.

Some design considerations for dynamic pressurization by explosions within piping are discussed by Antaki [7] and the specific problem of high explosive detonation inside vessels is discussed as background [9, 10] for the ASME Code Case 2564 on impulsively loaded vessels. Although elements of this Code Case apply to detonations inside piping, there are some essential differences which still need to be addressed, and at present there is no accepted Code Case or design guide for piping systems with internal detonations.

A detonation or shock wave propagating within a tube represents a traveling load in the form of a step or jump in pressure followed by an expansion wave. For ideal detonations, the wave speed is constant and approximately equal to the Chapman-Jouguet (CJ) value and the pressure loading is axisymmetric. A sudden load traveling at a constant speed excites periodic flexural waves [11] behind the wave front and the largest deformations are produced in the circumferential direction (hoop strain). The magnitude of the hoop strains has been extensively characterized in previous studies with straight tubes [11, 12].

Industrial piping systems are more complex than a simple straight pipe and typically include bends, tees, and closed ends (e.g., closed valves). When a detonation wave encounters a closed end, a reflected shock wave is created when the flow following the detonation wave comes to rest. Previous investigations [13, 14] have shown that the peak pressure of this reflected shock wave can be as high as 2.5 times the CJ pressure. The shock pressure rapidly decays as the wave moves away from the closed end. One consequence of this is a sudden jump in force in the direction perpendicular to the closure, which creates longitudinal (axial) stresses. As the shock propagates away from the closed end, flexural waves are also created in the tube just as in the case of the incident detonation wave. These two sets of flexural waves interfere, leading to the maximum strain values being observed at times corresponding to the passing of the reflected wave [11, 14].

When a detonation wave propagates through a bend, the change in direction of the flow results in the generation of a reaction force in the plane of the bend and opposing the resultant of the momentum flux of the flows into and out of the bend. In addition, the detonation wave diffracts, resulting in lower pressures on the inside (intrados) of the bend and higher pressures on the outside (extrados) of the bend. The detonation takes some time to recover from this disturbance and this results in an asymmetric loading downstream of the bend. The net consequence of the propagation through a bend is a time-dependent force on the elbow that has an impulsive and a static component. These forces and impulses generate structural motion in a piping system, resulting in primarily bending motions. One of the key issues is the possibility that the hoop and bending deformations occur simultaneously, which will complicate the evaluation of the structural loading. When a

detonation wave propagates into a tee junction, the effect is similar to that with an elbow but the direction and magnitude of the force is different.

The net result is that as the detonation propagates through the piping system, a series of forces are applied at the bends, tees, and closed end as shown in Figure 1. As shown in the figure, the detonation arrives at each location after some propagation delay and then the time-dependent loading is suddenly applied.

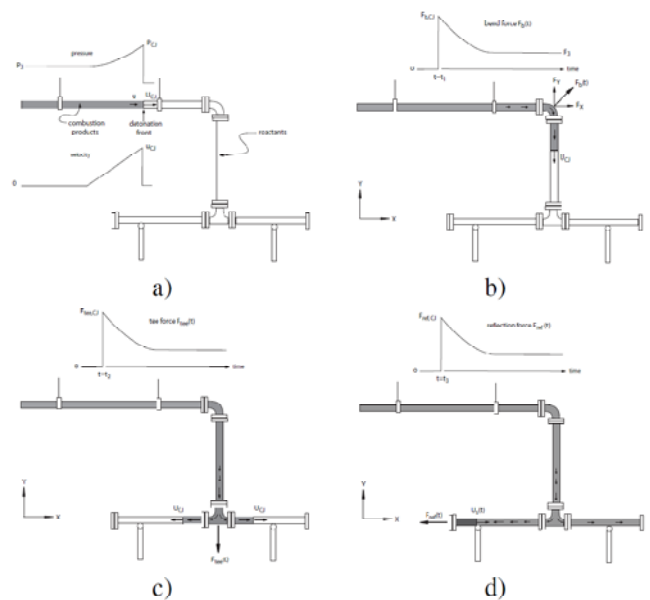


Figure 1. Generation of Structural Loads due to a) Detonation Propagation, and Interactions with b) Bends, c) Tees, and d) Dead Ends

The focus of this study are the forces that are developed at 90° bends. There is currently very little experimental data available to guide the analysis of piping systems with bends to internal detonations. Thomas [15] performed experiments in three piping systems fabricated from GRP and MDPE and measured strains, displacements, and pressures at selected points. However, data from experiments conducted in piping systems using more applicable pipe sizes, configurations, and materials for industrial applications are not available. The goal of this work is to develop pressure time-histories that can be used in finite-element model simulations to predict the structural response of piping systems subject to gaseous detonations for design and safety analyses without performing detailed computational fluid dynamics analyses. Laboratory testing was performed to gather experimental strain data in the hoop and axial direction, and both simple models and detailed finite-element modeling were used to validate the pressure time-histories considered.

Experimental Apparatus and Description

The test apparatus was a 2-inch schedule 40 piping system constructed from ASTM A312 type 304 stainless steel

with a nominal 3.8 mm (0.154 in.) wall thickness [16]. The piping system was composed of a horizontal section approximately 1.5 m long, a single 90° bend with a 19.3 cm bend radius, and a vertical section approximately 1.5 m long (see Figure 2). Class 300 lb slip-on flanges were welded to the two ends of the pipe. Two configurations were tested. The first fixed both ends of the pipe by bolting the flanges to large steel brackets that were fastened to steel plates bolted to the laboratory walls. In the second configuration the steel bracket was replaced with a short (179 cm long) steel cantilever beam, to allow measurement of the reaction loads, that was captured in a second bracket using dog screws that were set to be just in contact with the cantilever beam. The cross-section of the shot cantilever was a 0.0254 mm (1 in.) by 0.0318 mm (1.25 in.) rectangle with the longer side aligned axially with the pipe. A picture of the short cantilever configuration is presented in Figure 3. All welding was certified to ASME B31.3 standards. Material properties for the system are included in Table 1.

The piping system was instrumented with bonded strain gages at selected locations to measure both the hoop and axial response of the pipe, and axial strain in two direction in the short cantilever beam in the second configuration. The strain gages were wired in quarter-bridges with Vishay 2310B signal conditioners operated in the wide band mode (140 kHz, -3 dB point). Pressure was measured using Piezo-electric pressure transducers (PCB 113A) placed along the side of the pipe and in the flange at the end of the pipe. All of the pressure and strain data was recorded using a 14-bit transient digitizer with a 1 MHz sampling frequency. Before each experiment, the piping system was evacuated to 40 mTorr and then filled with the test mixture of 30% hydrogen and 70% nitrous oxide using the partial pressure method. Once the pipe had reached 1 atm, the mixture was circulated through the system using a bellows pump connected to each end. The pump was run until the volume of the system has been circulated at least 5 times. Once the valves were closed to the circulation loop, the mixture was ignited using an ordinary spark plug located at the horizontal end of the pipe. In order to achieve ideal detonations, a short (305 mm) Shchelkin spiral was inserted into the beginning of the horizontal section to increase turbulence generation such that the flame quickly accelerated up to a detonation. The gas properties for 30 H₂ and 70 N₂O detonations are included in Table 2.

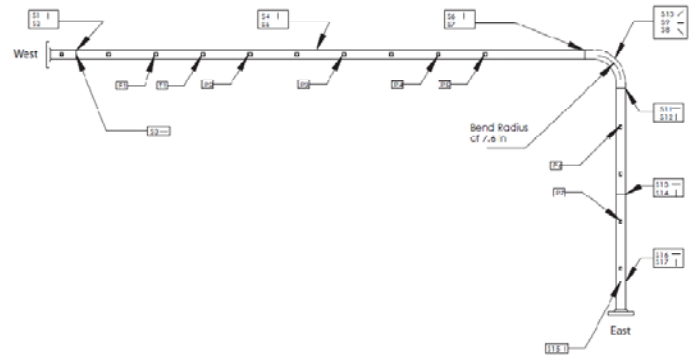


Figure 2. Experimental Setup with Sensor Locations

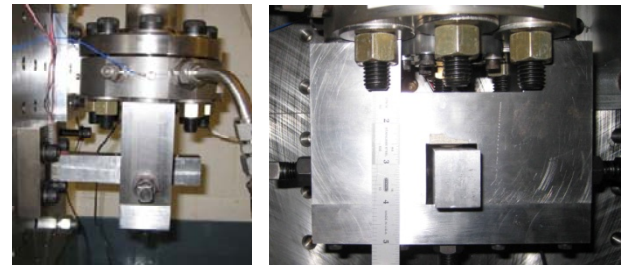


Figure 3. Pictures of Short Cantilever Beam Setup

Table 1. 2-in. Schedule Type 304 Stainless Steel Pipe Properties

Outer Diameter (OD)	60.3	mm
Inner Diameter (ID)	52.5	mm
Thickness (<i>t</i>)	3.91	mm
Mean Radius (<i>R</i>)	28.2	mm
Pipe Young's Modulus (<i>E</i>)	1.95×10^{11}	Pa
Pipe Mass Density (ρ)	8040	kg/m ³
Pipe Poisson's Ratio (ν)	0.31	
Hoop Frequency ($f_{breathing}$)	29	kHz
Flexural Frequency ($F_{flexural}$)	3.1	kHz

Table 2. 30% H₂ 70% N₂O Mixture Properties at Each State as Computed with the Shock and Detonation Toolbox [17].

Initial Conditions		
Pressure	100	kPa
Temperature	295	K
Density	1.28	kg/m ³
CJ State		
Wave Speed (U_{CJ})	2088	m/s
Pressure (P_{CJ})	2.63	MPa
Temperature (T_{CJ})	3383	K
Sound Speed (c_{CJ})	1142	m/s
Post-Expansion State		
Pressure (P_{CJ})	0.958	MPa
Temperature (T_3)	3005	K
Sound Speed (c_3)	1107	m/s
Reflected Shock		
Pressure	6.53	MPa

Experimental Results

A total of 36 shots were carried out including replicate shots to show test-to-test repeatability and shots using slightly different pipe configurations. In this paper we will focus primarily on the data from Shot 3, the first configuration with both ends of the pipe fixed, and Shot 32, with the short cantilever beam installed at the east end.

Shot 3 Results

The pressure and strain data are shown in Figure 4, Figure 5, and Figure 6. The detonation velocity was determined from the arrival time at each transducer and was found to be within 1% of the values reported in Table 2. The detonation pressures were also consistent with the CJ detonation pressure and a reflected peak pressure of approximately 2.5 times the CJ detonation pressure was measured at P8.

As indicated in Figure 1, S1, S4, S6, S11, S13, and S16 measure hoop strain in the pipe and S2, S3, S5, S7, S9, S12, S14, S15, and S17 measure axial strain in the pipe. Strain gages S8 and S10 are located on the bend and oriented at 45° relative to the hoop and axial direction. Peak strains in the hoop direction were between 200 and 300 μ strain. These strains are consistent with a dynamic load factor (DLF) of 2 to 2.5 applied to the CJ detonation pressure using a single degree of freedom harmonic oscillator to model the radial response of the pipe.

Peak axial strains in the straight pipe ranged from 100 and 200 micro strain, with a peak axial strain of 330 micro

strain occurring at S9 on the bend. Unlike the hoop response, the axial response of the pipe is not dominated by a single mode. Rather, multiple modes contribute to the axial response including localized through-wall bending modes, uniaxial extensional modes, and macro pipe bending modes. In addition to these axial modes, flexural modes are excited as the bend tends to ovalize as it is pressurized. Each of these modes is discussed in detail in the following sections.

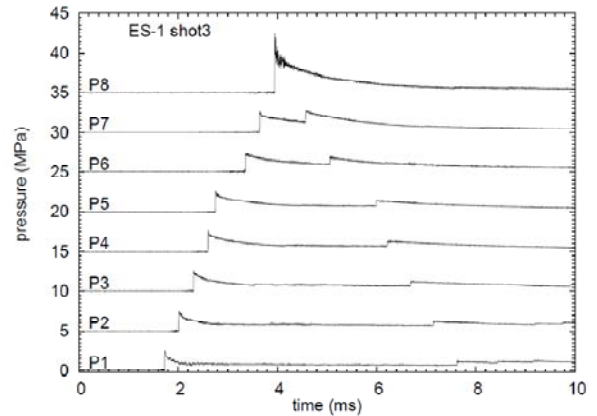


Figure 4. Shot 3 Pressure Measurements

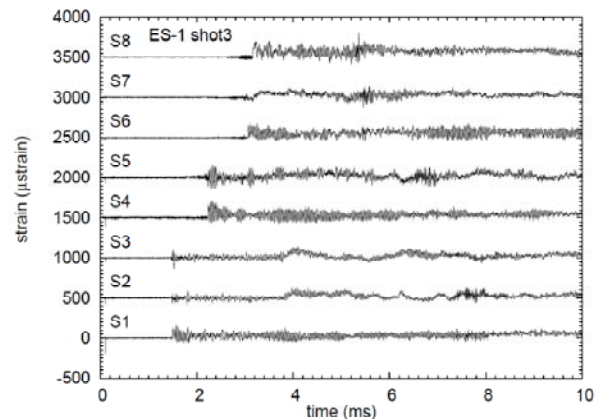


Figure 5. Shot 3 Strain Measurements (Set 1)

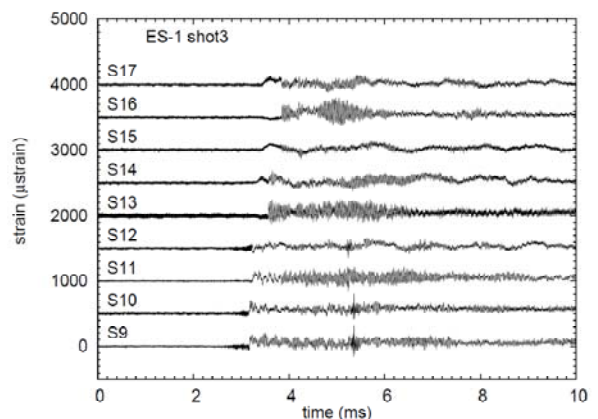


Figure 6. Shot 3 Strain Measurements (Set 2)

Through-wall Bending Modes

When a detonation propagates through a straight pipe, the radial response of the pipe generally oscillates at the fundamental breathing mode, which can be calculated [18] using Equation (1).

$$f_{\text{breathing}} = \frac{1}{2\pi R} \sqrt{\frac{E}{\rho(1-\nu^2)}} \quad (1)$$

Although the pipe responds at approximately the breathing frequency, the modal response itself is not the fundamental breathing mode where the entire pipe oscillates in phase radially. In reality the pipe forms a local bulge centered over the detonation wave front, and as the detonation propagates down the pipe, a series of oscillating bulges are left in its wake. A snapshot in time of the finite-element simulation discussed later is provided as Figure 7 to illustrate this phenomenon. Figure 7 includes outer surface axial stress contours to highlight the through-wall bending of the pipe. At the maximum outward radial excursions, the axial stress is positive, and at the minimum radial excursions the axial stress is negative.

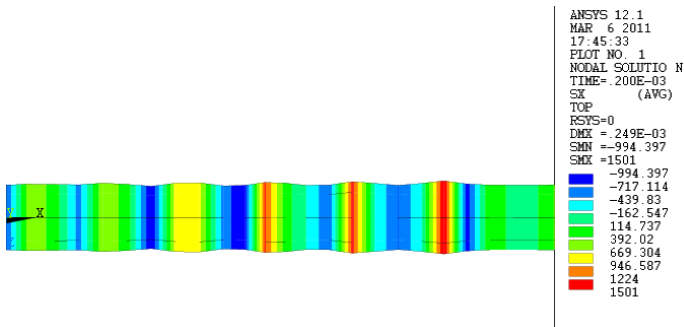


Figure 7. Through-wall Bending Mode Shape from Detonation Analysis Including OD Axial Stress Contours

The through-wall bending of the wall is a result of the radius of curvature of the bulge. As a result, the axial strains also include a response at the fundamental breathing frequency of the pipe that is not only a result of Poisson coupling with the hoop stresses. Poisson coupling would be expected to produce stresses of the opposite sign as the hoop stress on the outer surface. However, the through-wall bending stresses are larger than the Poisson component from the hoop stress such that the axial stresses on the outer surface are in phase with the hoop stresses. This is confirmed by the test data in Figure 8 where the hoop and axial response at S4 and S5 (upstream of the bend) are nearly in phase just after the arrival of the detonation at these locations and before any interactions with the bend. It is further noted that the through-wall bending axial strains shown in Figure 8 are of the same order of magnitude as the hoop strains.

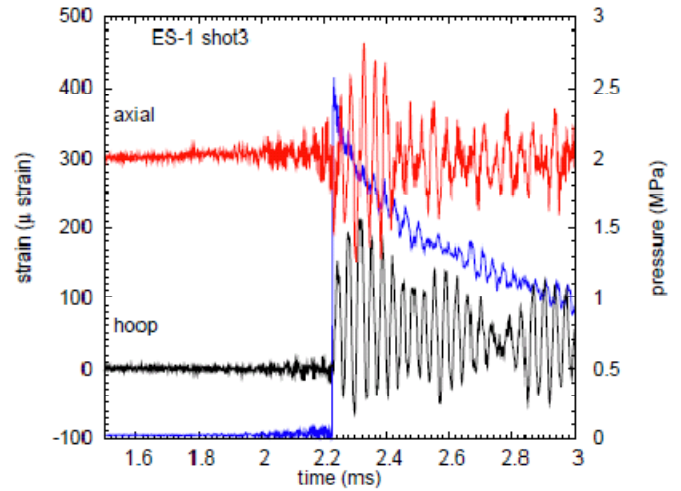


Figure 8. Comparison of hoop and axial strains excited by initial detonation waves.

Extensional and Macro Pipe Bending Modes

When the detonation propagates around the bend, an unbalanced load is developed. The pressures and flow through bend are unsteady and the direction of the load changes as the detonation traverses the bend. The net load causes the bend to displace outwards pulling on the horizontal and vertical straight pipes. This outward load produces an extensional bar wave that propagates away from the bend at the longitudinal wave speed in the pipe. The longitudinal (bar) wave speed [19] is calculated to be 4900 m/s using Equation (2) which is faster than the detonation itself.

$$c_0 = \sqrt{\frac{E}{\rho}} \quad (2)$$

The bar wave can be observed to run out ahead of the detonation wave as it propagates down the vertical pipe in Figure 6. The first clear sign of the bar wave is at S14. The initial tensile excursion from the bar wave at approximately 3 ms precedes the higher frequency oscillations from the radial response of the pipe excited by the detonation itself by approximately one quarter of a millisecond. At S15 and S17, the bar wave is even further ahead of the high frequency response from the arrival of the detonation. A closer view of the bar wave at S15 and S17 is shown in Figure 9. The bar wave looks identical at S15 and S17. Because these strain gages are collocated axially, although circumferentially offset by 90°, with S15 located on the front face of the pipe in the view shown in Figure 2 and S17 located on the right hand side of the vertical pipe, Figure 9 further supports that the initial response observed at S14, S15, and S17 is a uniaxial bar wave. It is noted that a bar wave also propagates down the horizontal

pipe, but because the detonation has already passed through this section of pipe, it is more difficult to observe. However, a bar wave could be observed in the horizontal section in tests where the gas was ignited from the lower end of the vertical section.

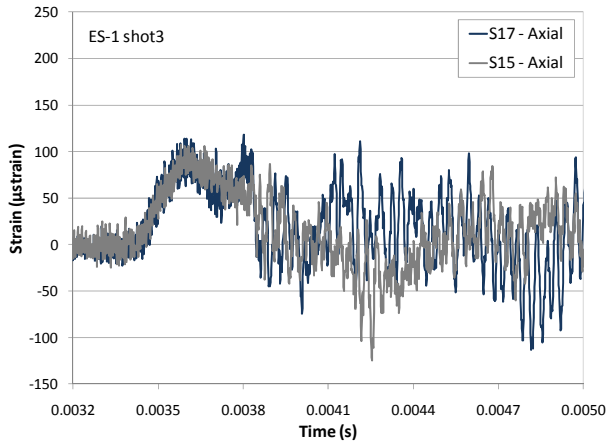


Figure 9. Axial Tension Wave at S15 and S17

After the passage of the bar wave, the response from the longer period macro pipe bending modes is observed in Figure 6. The frequencies of the excited modes are highly dependent on the geometry of the piping system itself, due to both the dependence of the frequency on the length of the pipe and the timing of the detonation wave loading each bend, and are more difficult to predict without performing finite-element simulations.

Flexural Ovalization Modes

Ovalization of bends is a well known phenomenon and has lead to creating flexibility factors for piping flexibility analyses [20] in order properly model the stiffness of the system. The expected ovalization frequency can be estimated by calculating the first flexural (ovalization) frequency in straight pipe [18].

$$f_{flexural} = \frac{\lambda_i}{2\pi R} \sqrt{\frac{E}{\rho(1-\nu^2)}} ; \lambda_i = \frac{1}{\sqrt{12}} \frac{t}{R} \frac{i(i^2-1)}{\sqrt{1+i^2}} \quad (3)$$

For 2-inch Schedule 40 pipe, the first flexural mode frequency is calculated to be 3100 Hz. It is difficult to see the ovalization response in the bend strain gage data (i.e., at S8, S9, or S10). Therefore, a fast Fourier transform (FFT) of the response at S10 was performed and is shown in Figure 10, which includes the FFT of the response predicted by the finite-element model at S10 discussed later for comparison. The strongest peak in Figure 10 is at the 29 kHz breathing mode frequency of the pipe, but a distinct peak is also at 4300 Hz which consistent with the expected first flexural mode frequency in straight pipe. The flexural mode is confirmed by performing a modal analysis of the finite-element model to determine the mode shape at 4300 Hz. The modal analysis

showed the numerous modes with flexural characteristics exist in this frequency range. An example flexural mode at 4260 Hz is shown in Figure 11.

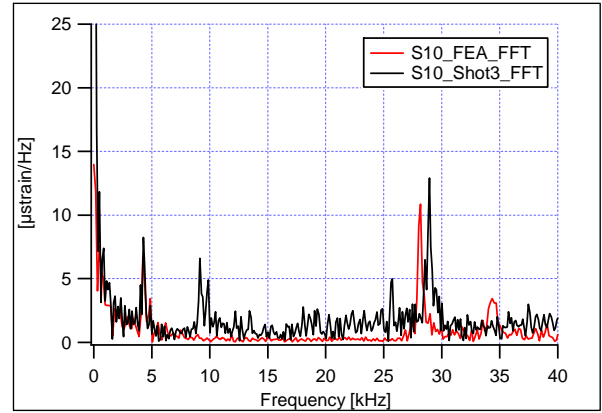


Figure 10. FFT of S10 from Shot 3 and FE Analysis

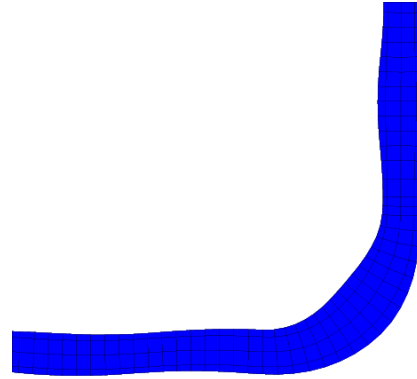


Figure 11. Example Flexural Mode Shape at 4260 Hz

Shot 32 Results

The overall effect of installing the short cantilever was negligible on the pressure and pipe strain data compared to Shot 3 and are not included in this paper. The strains measured on the short cantilever are shown in Figure 12. S24 is oriented to measure axial loads (with respect to the pipe) and S25 is oriented to measure lateral loads. The dog screws connect to the cantilever 114 mm (4.5 in.) from the fixed end of the cantilever and the strain gages are located 25 mm (1 in.) above the fixed end. The maximum forces can be estimated from these strains (assuming the cantilever is responding quasi-statically) by rearranging the bending equations to the following form where the applied load is calculated from the measured strain:

$$P = \frac{\epsilon E_b I}{Lc} \quad (4)$$

where E_b is the modulus of elasticity of the beam (2×10^{11} Pa), I is the second area moment of the beam, L is the effective length from the applied load to the strain gage, c is distance from the bending axis to the outer surface where the strain gage is located, and ε is the measured strain. For the maximum measured strain in the axial direction (S24) of approximately 200 μ strain, the maximum axial load is calculated to be 1950 N (440 lbs).

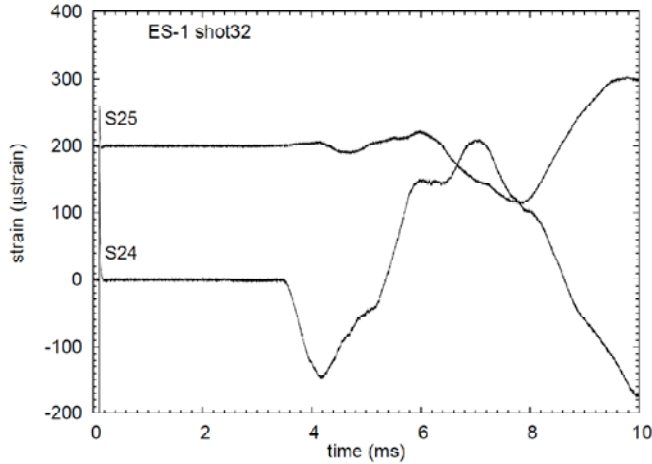


Figure 12. Shot 32 Short Cantilever Strains – S24 Oriented to Measure Axial Loads

Detonation Modeling

The detonation pressure, velocity, and density throughout the expansion fan behind the detonation front can be solved for explicitly, and is referred to as the Taylor-Zel'dovich (TZ) or Taylor wave. The spatial and temporal distribution of pressure, velocity, and density throughout the pipe are given by Equation (5), (6), and (7) below [21].

$$P_{det}(x,t) = \begin{cases} P_1 & U_{CJ} < x/t < \infty \\ P_3 \left[1 - \frac{\gamma_2 - 1}{\gamma_2 + 1} \left(1 - \frac{x}{c_3 t} \right) \right]^{\frac{2\gamma_2}{\gamma_2 - 1}} & c_3 < x/t < U_{CJ} \\ P_3 & 0 < x/t < c_3 \end{cases} \quad (5)$$

$$\rho(x,t) = \begin{cases} \rho_1 & U_{CJ} < x/t < \infty \\ \rho_3 \left(\frac{P(x,t)}{P_3} \right)^{\frac{1}{\gamma_2}} & c_3 < x/t < U_{CJ} \\ \rho_3 & 0 < x/t < c_3 \end{cases} \quad (6)$$

$$u(x,t) = \begin{cases} 0 & U_{CJ} < x/t < \infty \\ \frac{2c_3}{\gamma_2 + 1} \left(1 - \frac{x}{c_3 t} \right) & c_3 < x/t < U_{CJ} \\ 0 & 0 < x/t < c_3 \end{cases} \quad (7)$$

The subscripts indicate states from which each parameter is evaluated. The subscript 1 indicates the initial state prior to the arrival of the detonation, 2 is the CJ state, and 3 is the post-expansion region, where the velocity of the reaction products has reached zero. The properties P_3 and c_3 are the pressure and speed of sound in the post-expansion region and are calculated as follows:

$$C_3 = \frac{\gamma_2 + 1}{2} C_{CJ} - \frac{\gamma_2 - 1}{2} U_{CJ} \quad (8)$$

$$P_3 = P_{CJ} \left(\frac{C_3}{C_{CJ}} \right)^{\frac{2\gamma_2}{\gamma_2 - 1}} \quad (9)$$

The ratio of specific heats γ_2 , speed of sound at the CJ state c_3 , and the detonation velocity U_{CJ} can be calculated using chemical equilibrium software, such as NASA's CEA [22] or the Shock and Detonation Toolbox [17].

Bend Force Modeling

When a detonation or shock wave propagates through a bend, the initially straight wave front will be modified by transversely moving shock and expansion waves as the flow is forced to turn to follow the curved surfaces of the bend [21, 23]. Associated with these waves will be spatial and temporal variations in the pressure within the bend that are not accounted for in the simple CJ-TZ model described above. These variations can be estimated with the use of computational fluid dynamics. However, for our purposes, we have used a much simpler approach based momentum conservation within a control volume surrounding the bend and using an idealized pressure time-history based on the TZ model [21].

Quasi-Steady Bend Force Model

The simplest model for computing the force on the bend is to neglect the interaction of the wavefront and focus on the flow behind the wave. If we have a short bend at the end of a much longer section of straight pipe, then the flow may be treated as quasi-steady (QS) within the bend, as in the standard models of bend force used in water hammer [24, 25]. Using the control volume shown in Figure 13 and assuming uniform flow over the entrance (1) and exit of the bend, the force exerted by the fluid on the bend is found [21] to be:

$$\vec{F} = \hat{x} A_1 [(P_1 - P_a) + \rho_1 u_1^2] + \hat{y} A_2 [(P_2 - P_a) + \rho_2 u_2^2] \quad (10)$$

The pressure, velocity, and density in this equation are functions of time as computed from the TZ model described above. In water hammer, the dominant contribution to the force is due to the pressure terms. In detonations, because the flow is sonic behind the wavefront, the terms corresponding to pressure differences and fluid motion are of comparable size.

Immediately after the detonation wave passes through the bend, the peak force will be obtained and has a magnitude of $\sim 2A\Delta P_{CJ}$ in both directions. This is twice as large as the usual estimates used in water hammer, for which the contributions ρu^2 from the fluid motion are negligible compared to ΔP . The force acts at 45 degreesⁱ as shown in Figure 13 and will decrease with increasing time as the detonation propagates away from the bend.

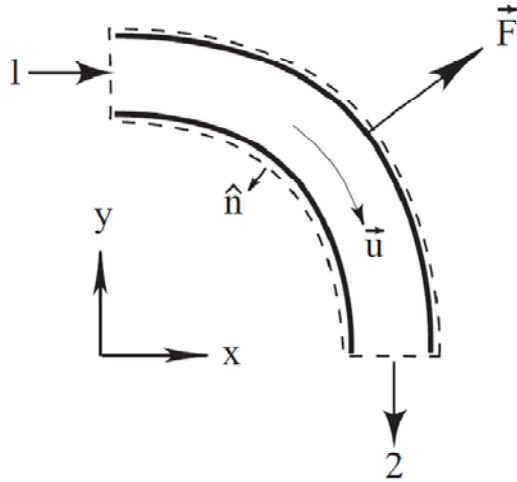


Figure 13. Bend fluid control volume for quasi-steady momentum theorem application.

Unsteady Idealized Bend Pressure Force Model

If we have a model for the wave front geometry and flow field inside the bend, then we can move the control volume to the inner surface of the pipe to compute a more refined estimate of the force. The geometry is shown in Figure 14.

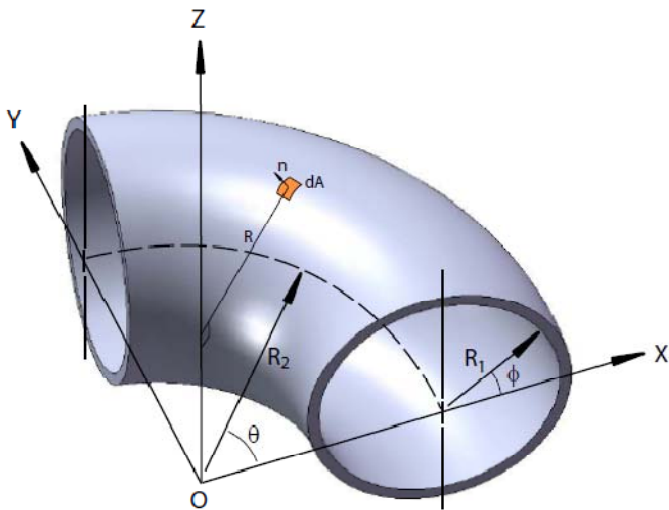


Figure 14 Geometry for integration of momentum integral using a control volume on the inner surface of the pipe and a detail model of the flow within the bend.

To account for the transient effects including wave motion through the bend, we apply the integral version of the momentum theorem, neglecting viscous forces on the bend walls since we are dealing with high speed flows that are dominated by inertial and pressure effects.

$$\vec{F} = \int_{\partial\Omega_1} [\rho \vec{u} \vec{u} \cdot \hat{x} + (P - P_a) \hat{x}] dA + \int_{\partial\Omega_2} [\rho \vec{u} \vec{u} \cdot \hat{y} + (P - P_a) \hat{y}] dA - \frac{d}{dt} \int_{\Omega_0} \rho \vec{u} dV \quad (11)$$

The quantities in the integral were computed using the TZ model together with the assumption that the wave front is flat and remains normal to the pipe wall while the fluid path lines are parallel to the pipe wall as the detonation propagates through the bend. Although this model is unrealistic, the measured pressure histories in a bend [23] indicate that the model pressure profiles are in reasonable agreement with the data except very close to the detonation wave front. The force-time history for the 90-degree bend in the present tests is shown in Figure 15. As expected, the quasi-steady model and the unsteady model compare quite favorably apart from the initial transient when the the detonation wave is within the bend.

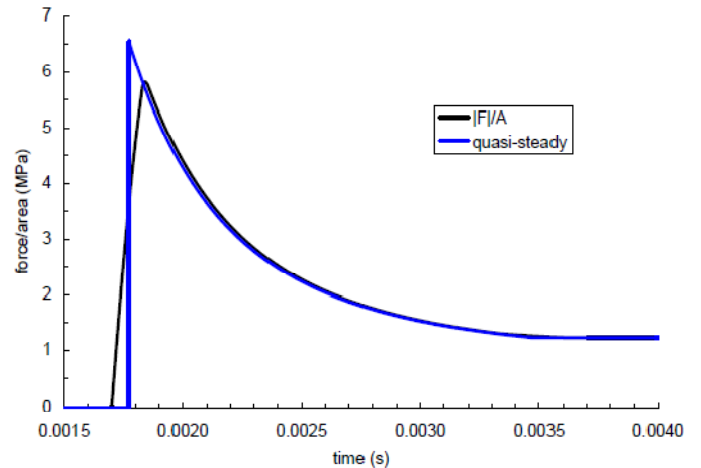


Figure 15 Comparison of the two methods of estimating the magnitude of the bend force (expressed as an equivalent pressure F/A) for the ES1 tests.

The models for the bend force have been validated against the experimental measurements using both simple analytical ideas about axial elastic wave propagation [21] as well as the finite element analysis described subsequently. The analytical modeling is instructive since it clearly shows the origin of the axial strain signal that precedes the detonation wave. Using the analytical solution for wave propagation in a bar and the force-time history estimated from the bend pressure force model, the strain history at the boths end of the piping

system has been computed and compared with the measured strains in Figure 16 (upstream of the bend) and Figure 17 (downstream of the bend).

The agreement of the timing, magnitude and overall strain history is quite reasonable and indicates that the basic physics of the axial strain pulse has been correctly identified.

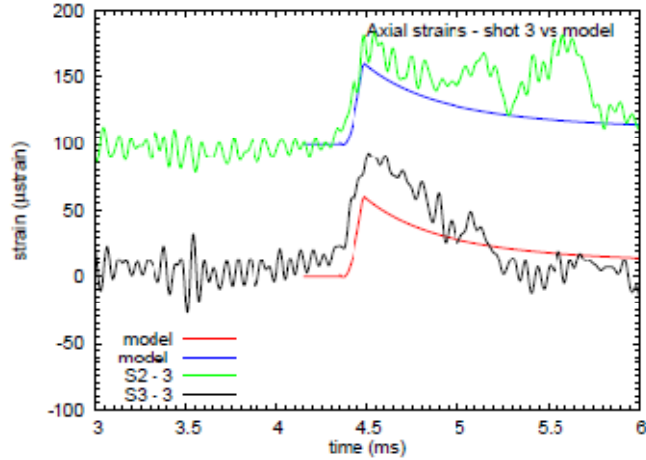


Figure 16 Comparison of filtered axial strain signals with analytic model based on bar wave propagation and estimated bend force. Upstream location.

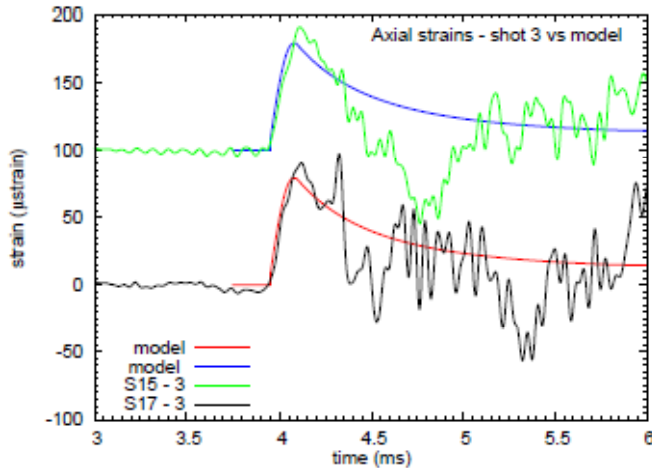


Figure 17 Comparison of filtered axial strain signals with analytic model based on bar wave propagation and estimated bend force. Downstream location.

Reflected Detonation Model

At the end of the pipe, the detonation reflects off the end flanges and a reflected shock propagates back into the pipe. An empirical model for the reflected detonation was developed based on the measured reflected detonation. The pressure behind the reflected shock uniformly decays as the gases expand away from the flange until the gas reaches the post-

expansion pressure P_3 . The pressure behind the shock was represented by the following double exponential:

$$P_{ref}(x,t) = \begin{cases} P_{det}(x,t) & U_{ref} < \frac{x}{t} < \infty \\ (2.5P_{CJ} - P_3) \frac{(e^{-t/T_1} + e^{-t/T_2})}{2} + P_3 & 0 < \frac{x}{t} < U_{ref} \end{cases} \quad (12)$$

The motivation for using the double exponential was to accurately capture both the rapid decay from the $2.5 \times P_{CJ}$ peak reflected pressure [13], calculated using the Shock and Detonation Toolbox [17], and the longer term decay to the post-expansion pressure. The time constants T_1 and T_2 were adjusted to fit the measured pressure data at P8 and their final values were 900 μ s and 120 , respectively, and the pressure time-history is compared to the P8 pressure data from Shot 3 in Figure 18. The reflected shock velocity U_{ref} , obtained from the arrival times at each pressure transducer, was taken to be 1,300 m/s.

The expression of Equation (12) is an empirical model that is based on experimental observations of pressure and validated for the piping model and explosive gases used in our tests. A more general approach is to consider the dynamics of the gases and the reflected shock wave that brings the flow to rest. The issues are discussed by Karnesky et al [14], who give a validated model that can be used for an arbitrary mixture and geometry.

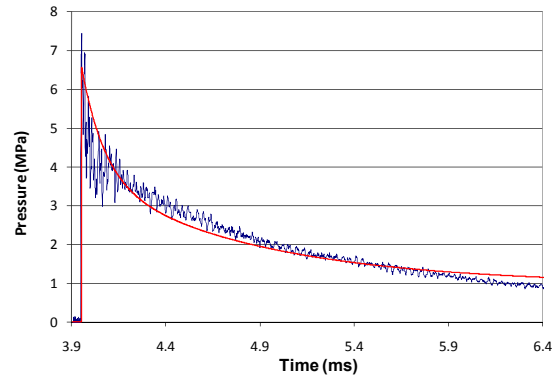


Figure 18. Reflected Detonation Model Compared to P8 from Shot 3

Finite-Element Modeling

Two finite-element models were constructed for these analyses. A half-symmetry finite-element model was created to simulate the pipe strain results from Shot 3. The model was constructed in ANSYS using 8-node shell elements (SHELL93), and the pipe was assumed to have a uniform nominal thickness. Four approximately square elements were used to describe the half-circumference of the pipe. The impact of the axial mesh refinement on the ability of the model to capture the through-wall bending axial stresses was also considered. The characteristic through-wall bending

wavelength in cylindrical shells can be shown to be $2\pi/\beta$, where Timoshenko [26] defines β as:

$$\beta^4 = \frac{3(1-\nu^2)}{R^2 t^2} \quad (13)$$

For the axial mesh refinement in these analyses, approximately two and a half elements (or six nodes) describe the through-wall bending wave length.

The model was constructed such that nodes were placed at the same locations as the strain gages in the experiments. At the two ends of the model, the shell nodes were coupled to a single pilot node located at the center of the pipe that was fixed in all six degrees of freedom. The model is shown in Figure 19.

The second model included the flanges, bracket, and short cantilever beam. The full 360° pipe was modeled using the 8-node shell elements and the flanges, bracket, and cantilever beam were modeled using beam type elements with the proper cross-section. The top of the cantilever was coupled to the bracket in the two in plane directions (x and z-direction in this case) and out of plane rotation (y-direction) to simulate the contact boundary condition between the short cantilever and the dog screws. The zoom-in of the model showing the short cantilever is provided as Figure 20.

At each time step the appropriate pressures were applied to the inner surface of the shell elements depending on their location in the pipe. The forward propagating detonation pressure in the straight pipe was applied using Equation (5) and Equation (12) was applied to the elements behind the reflected shock (i.e., after the detonation reaches the bottom of the vertical pipe and reflects back).

Within the bend, the internal pressure given by the planar wave TZ model has to be augmented to mimic additional momentum transfer associated with fluid motion. We developed two models for this purpose: 1) a quasi-steady (QS) model; and 2), an unsteady idealized (UI) model. The QS model assumes that the flow is steady through the bend. Therefore, the necessary applied pressure takes on a uniform amplification around the circumference of the bend above the TZ detonation pressure. The amplified pressure is described by one of the two components in Equation (10) (either \hat{x} or \hat{y}) divided by A , the area of the pipe. This amplified pressure is swept through the bend assuming the detonation remains planar.

The UI model varied the pressure around both the circumference of the bend and along its length. The following pressure distribution (using the variable definitions in Figure 14) was assumed based on previous bend pressure measurements [23]:

$$P_{UI}(x, \theta, \phi, t) = [1 + a \sin(2\theta) \cos(\phi)] P_{det}(x, t) \quad (14)$$

An analytical solution for the amplification factor a was determined by evaluating the surface integrals in Equation (11) using the assumed pressure distribution and equating the resulting force to the quasi-steady solution, Equation (11). The result, Equation (15), is an analytical expression for the parameter a which depends on location and time.

$$a = \frac{3}{2} \frac{R_1}{R_2} \left[\frac{\rho(x, t) u^2(x, t)}{P_{det}(x, t) - P_a} \right] \quad (15)$$

In the finite element models, this result was used by applying a pressure to each element in the bend based on its location using Equation (14) and Equation (15) with flow properties from the planar TZ solution. For both bend force analysis methods, once the wave front reached the end of the bend, the pressure applied within the straight pipe was the TZ detonation equations.

The implicit time integration analysis used a time step equal to 1/20 the breathing mode period calculated using Equation (1), and the analysis simulated 7.6 ms of response. No damping was assumed, due in part to the limitations of Rayleigh damping where damping can only be specified at two frequencies.

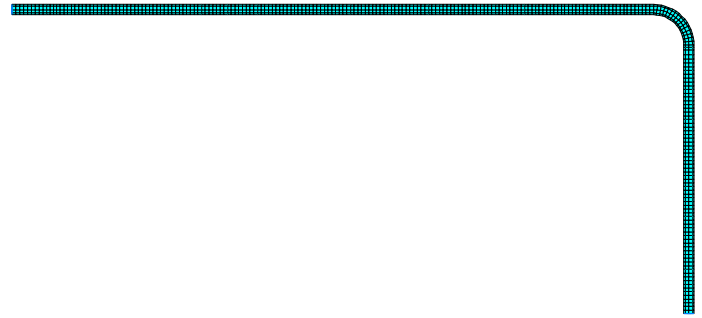


Figure 19. Fixed Ends Half-Symmetry Finite-Element Model

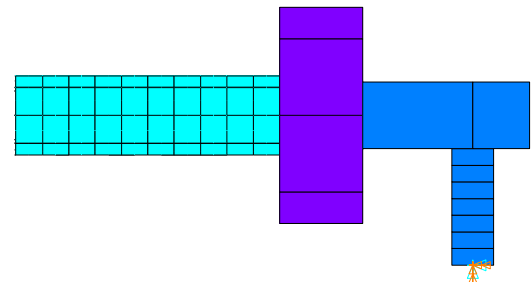


Figure 20. 360° Finite-Element Model Showing Short Cantilever Connection

Finite-Element Pipe Strains

The strains predicted by the finite-element model at the strain gage locations using the Simplified Control Volume (QS) and Pressure Variation (UI) bend pressure distributions are compared to the measured strains from Shot 3. It is noted that the finite-element strain results in these figures are shifted

forward in time by 1.4 ms to line up with the measured strain data.

The hoop strains from the two models are approximately the same because the detonation and reflected detonations used in the two analyses were the same. The FFT of S10 in Figure 10 shows that the breathing frequency is slightly under-predicted at 28 kHz versus 29 kHz. Selected hoop strains are compared in Figure 21 through Figure 24. In general, the hoop strains show good correlation with the most significant under-prediction being observed at S16 in Figure 24. The trends in the strains predicted by the models are good although the details are not identical. The response predicted by the model at S1 attenuates at a similar rate to the data shown in Figure 21, but between 3 ms and 7 ms the predicted response is significantly lower. The predicted response correlates better with the data at S4 and S13 where there are periods of both over and under-prediction.

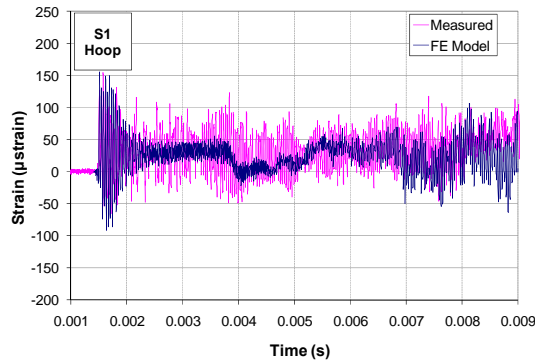


Figure 21. Comparison of QS Analysis to Shot 3 Data at S1

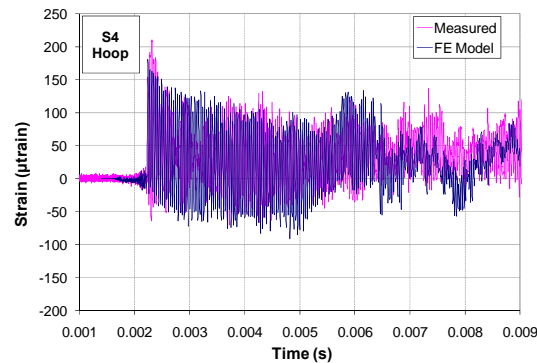


Figure 22. Comparison of QS Analysis to Shot 3 Data at S4

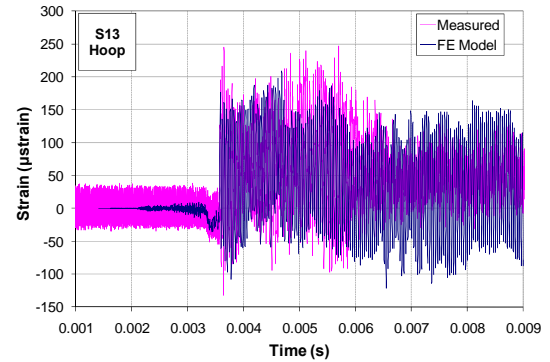


Figure 23. Comparison of QS Analysis to Shot 3 Data at S13

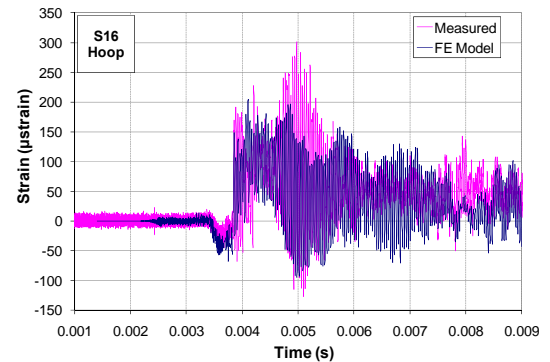


Figure 24. Comparison of QS Analysis to Shot 3 Data at S16

The axial strains from the finite-element models using the QS and UI bend pressure models are compared side-by-side in Figure 25 through Figure 38 in the following pages. Both models produce results that are consistent with the data. The first 2 ms of response shows the best correlation with the test data from Shot 3. The best correlation is observed near the bend, in particular at S7 shown in Figure 27 and Figure 30. The bar wave is clearly reproduced by the model, but it is notably over-predicted at S15 and S17. At S2 and S3, the bar wave appears to be over-predicted by a lesser margin than at S15 and S17, although the high frequency through-wall bending stress component slightly obscures the interpretation. This result would imply that the resultant bend force may not be centered at 45° around the bend. The over-prediction of the bar wave and gross bending stress is not entirely unexpected. The shell nodes are constructed at the mid-radius of the pipe such that the pressure applied over a greater area than in the actual pipe. However, this is only expected to be an ~15% effect.

The most significant differences between the two bend pressure distribution models is observed in the axial strains measured in the bend at S9 (see Figure 31 and Figure 35). The axial strain from UI model are clearly more consistent with the measured strains, although the results from both bend pressure distribution models generally under-predict the response. However, the ovalization response is captured by the model and

the FFT of S10 in Figure 10 shows that response frequency is almost identical to the measured response frequency.

The high frequency through-wall bending stress component in all of the comparison plots is generally under-predicted. The under-prediction also doesn't appear to correlate with under-prediction of the hoop strains measured at the same axial location. This could be a result of the nominal uniform wall thickness assumption. Analyses have shown

that variations in the wall thickness can have a significant effect on the stresses in the pipe [12]. At later times, the differences between the predicted response and the measured strains begin to increase, but the overall trends are consistent. The lack of damping assumed in the model may be contributing to these differences, but overall, the two bend pressure distribution models adequately predict the response.

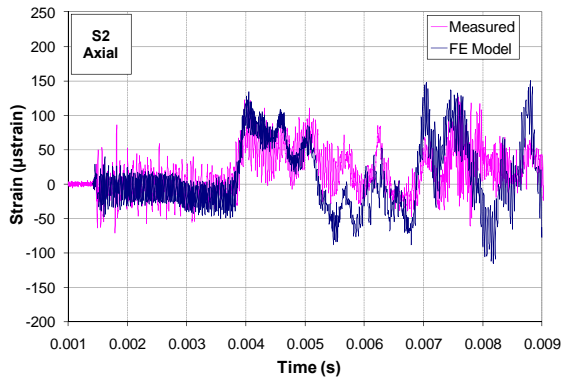


Figure 25. Comparison of QS Analysis to Shot 3 Data at S2

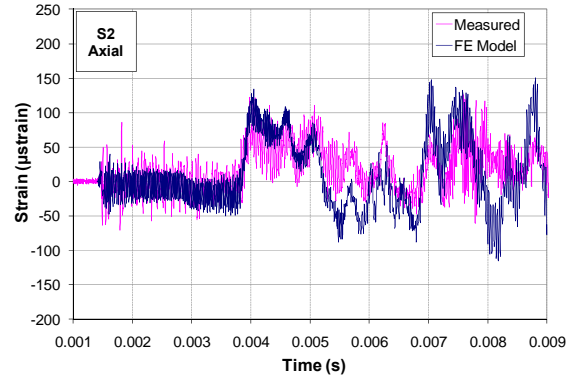


Figure 28. Comparison of UI Analysis to Shot 3 Data at S2

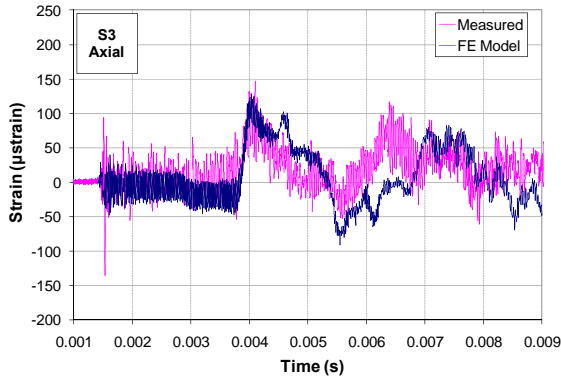


Figure 26. Comparison of QS Analysis to Shot 3 Data at S3

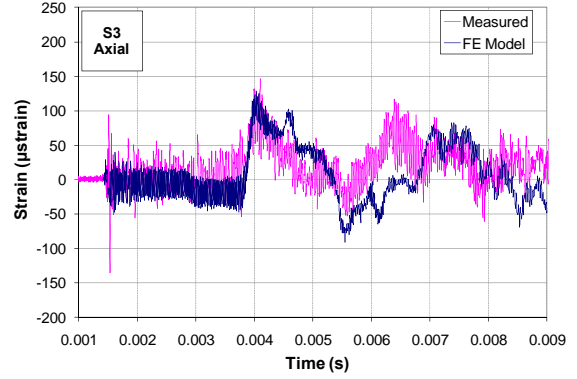


Figure 29. Comparison of UI Analysis to Shot 3 Data at S3

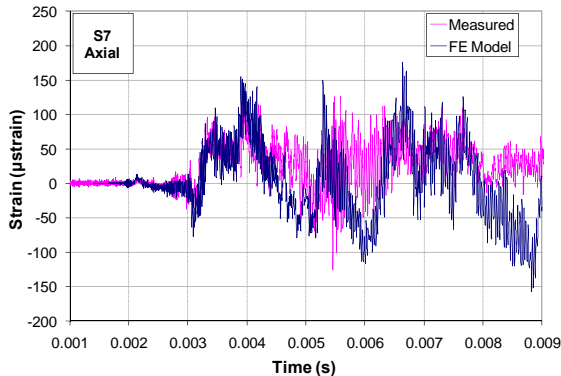


Figure 27. Comparison of QS Analysis to Shot 3 Data at S7

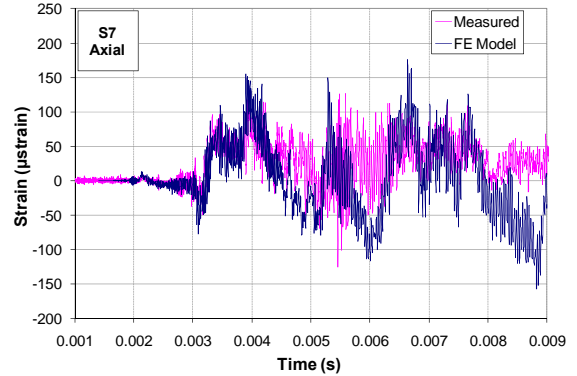


Figure 30. Comparison of UI Analysis to Shot 3 Data at S7

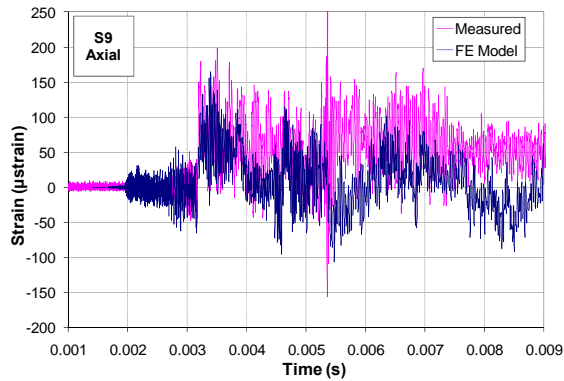


Figure 31. Comparison of QS Analysis to Shot 3 Data at S9

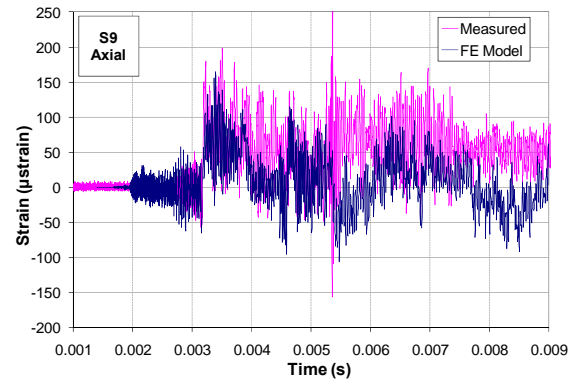


Figure 35. Comparison of UI Analysis to Shot 3 Data at S9

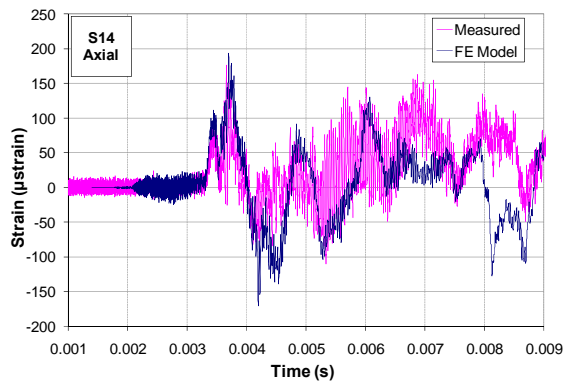


Figure 32. Comparison of QS Analysis to Shot 3 Data at S14

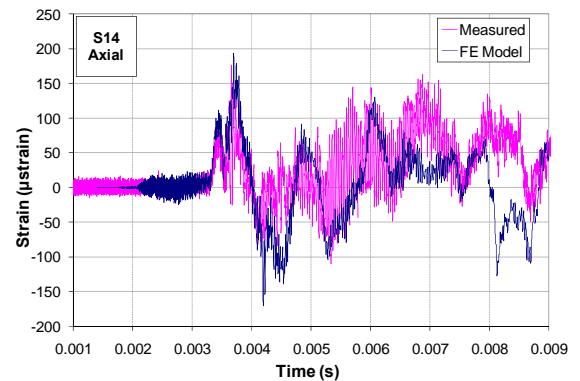


Figure 36. Comparison of UI Analysis to Shot 3 Data at S14

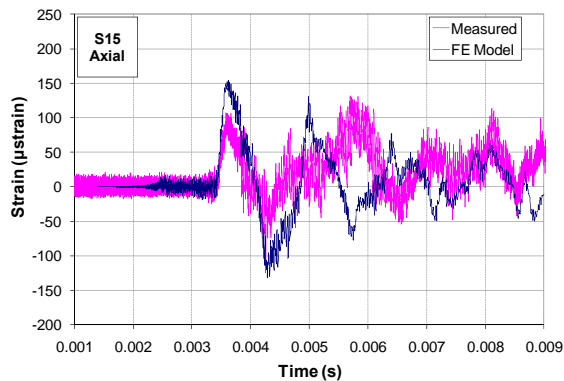


Figure 33. Comparison of QS Analysis to Shot 3 Data at S15

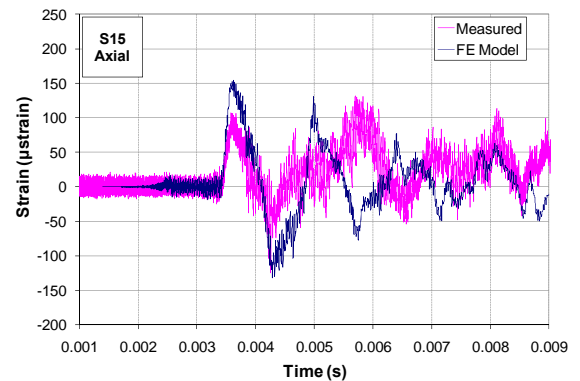


Figure 37. Comparison of UI Analysis to Shot 3 Data at S15

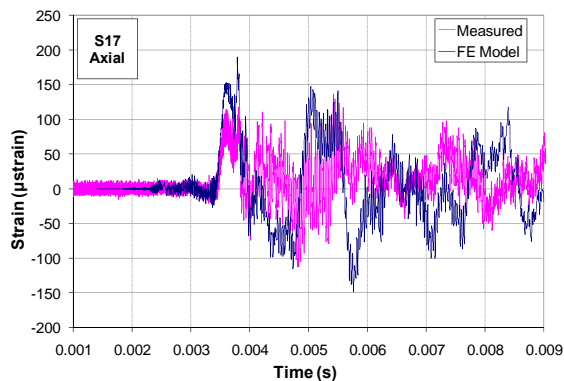


Figure 34. Comparison of QS Analysis to Shot 3 Data at S17

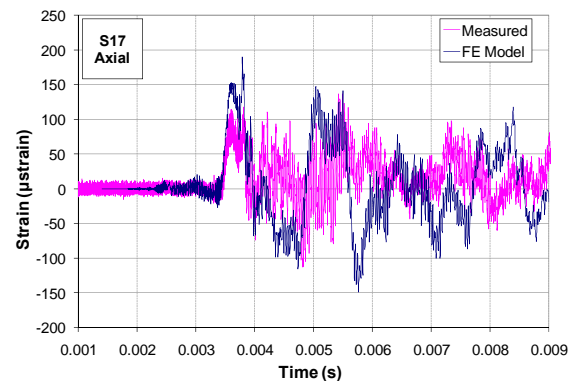


Figure 38. Comparison of UI Analysis to Shot 3 Data at S17

Finite-Element Reaction Loads

The reactions forces from the two bend pressure models at the two fixed nodes at the ends of the fixed finite-element model are compared in Figure 39 through Figure 44. Similar to the pipe strain results, there are few differences in the reaction forces from the UI and QS models. However, it is interesting to note the differences between the reaction forces at the two ends of the model.

The axial force at the ignition end on the horizontal segment initially jumps up due to the post-expansion pressure P_3 . The force from the detonation pressurizing the bend doesn't reach the ignition end until almost 3 ms later. At the other end where the reflection occurs, the forces are significantly higher due to the combined effect of the detonation initially pressurizing the bend and then the detonation reflected off the flange. The lateral forces at the two ends are of similar magnitude and are significantly reduced compared to the axial forces. The magnitude of all the forces, however, is significantly higher than the forces estimated from the strains measured in the short cantilever.

The strains in the short cantilever (S24, S25) from the second finite-element model are compared to the measured strains in Figure 45. The finite-element model strains over-predict the measured strains by more than a factor of two. However, the finite-element model strains are significantly less than the strain that would have been expected based on the forces that were predicted by the fixing the end of the model. Therefore, the flexibility of the short cantilever did significantly reduce the reaction forces. The frequency of the predicted response is consistent with the measured strain which suggests that the modeling assumptions are appropriate (i.e., the stiffness and masses are approximately correct). The over-prediction is significantly larger than the over-prediction that was observed in the pipe strains. This may suggest that the load transfer from the bracket through the dog screws to the cantilever may not be ideal. Although the model does not appear to precisely predict the reaction loads, the results are conservative.

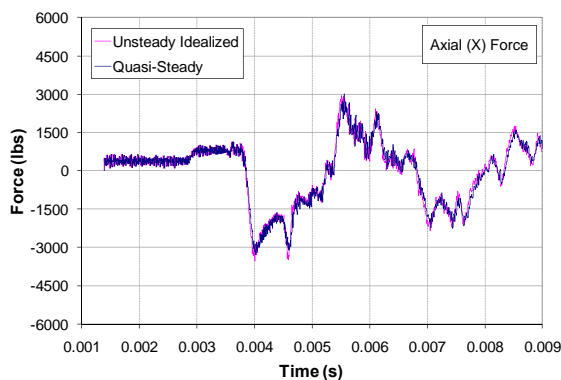


Figure 39. Comparison of UI and QS Axial (X) Reaction Forces at Ignition (Horizontal) End

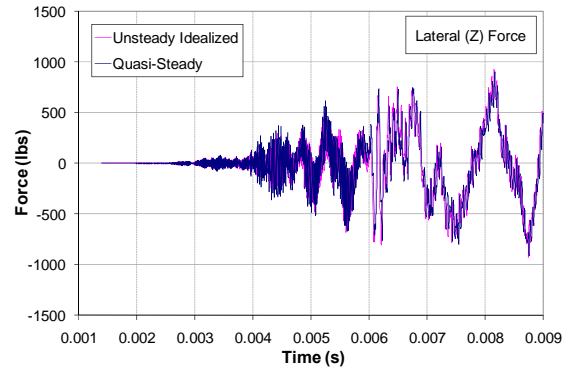


Figure 40. Comparison of UI and QS Lateral (Z) Reaction Forces at Ignition (Horizontal) End

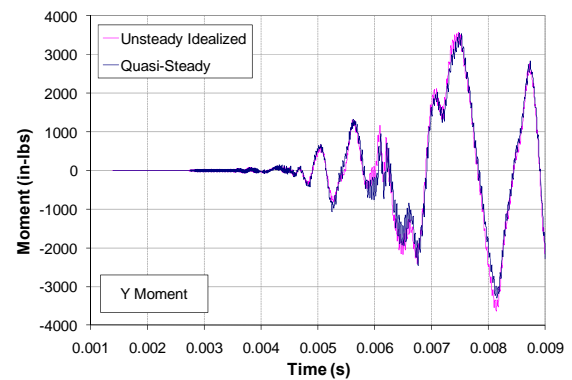


Figure 41. Comparison of UI and QS Out-Of-Plane (Y) Reaction Moments at Ignition (Horizontal) End

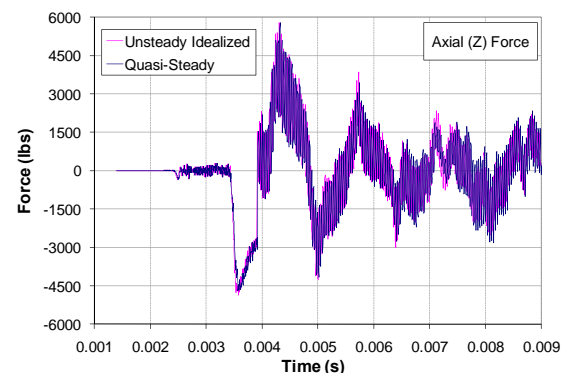


Figure 42. Comparison of UI and QS Axial (Z) Reaction Forces at Reflection (Vertical) End

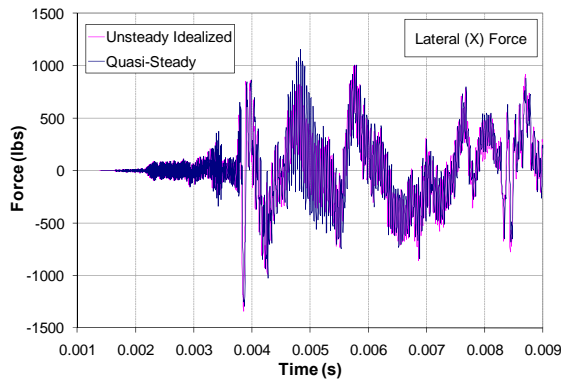


Figure 43. Comparison of UI and QS Lateral (X) Reaction Forces at Reflection (Vertical) End

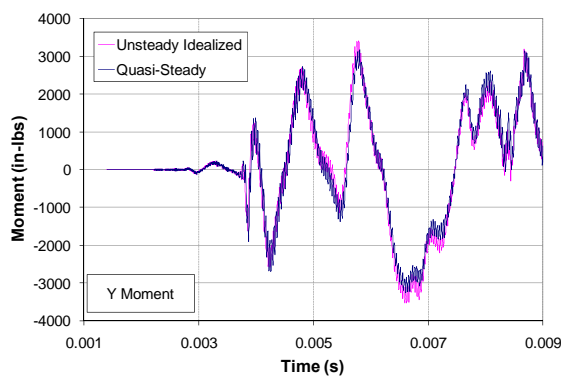


Figure 44. Comparison of UI and QS Lateral (X) Reaction Forces at Reflection (Vertical) End

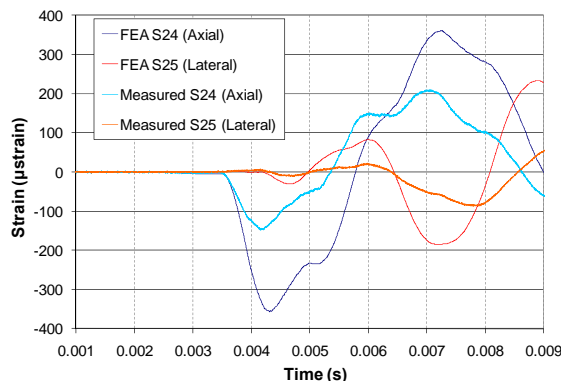


Figure 45. Comparison of UI FEA and Measured Short Cantilever Strains (S24, S25)

CONCLUSIONS

A time-dependent force is generated when a detonation passes through a bend. The origin of the bend force can either be visualized as the change in momentum of the flow behind the detonation wave or the distribution of pressure inside the bend as the wave front changes direction within the pipe. The time-dependent force generates a longitudinal stress wave in the piping that can be observed on the strain gauges and is predicted by both analytical models and finite element simulations. The peak magnitude of the bend force is

approximately twice that due to the pressure alone since the peak momentum flux of the flow behind the detonation front is comparable to the pressure in the front.

The forces that are produced at bends can be estimated by applying the conservation of momentum equations to control volumes drawn around the bend. These analyses can be used to develop bend pressure distributions that can be applied to shell finite-element models to attain satisfactory predictions of the strains measured in the adjoining straight pipe. The strains in the bend itself were not studied in detail and it is unclear whether these simplified bend pressure distribution models will produce satisfactory results in the bend itself. Reaction loads appear to be more difficult to predict, but the finite-element simulations tend to over-predict the response such that the models are still appropriate for safety analysis and design.

ACKNOWLEDGEMENTS

We acknowledge the very substantial contributions of Dr. Raza Akbar in designing the ES-1 specimen as well as constructing and operating the test facility at Caltech. The work described in this paper was performed in support of the U.S. Department of Energy's (DOE's) Hanford Tank Waste Treatment and Immobilization Plant (WTP) Project (contract number DE-AC27-01RV14136), under subcontract to DOE prime contractor Bechtel National, Inc.

REFERENCES

- [1] Ciccarelli, G., and Dorofeev, S., 2008, "Flame acceleration and transition to detonation in ducts," *Progress in Energy and Combustion Science*, 34(4), pp. 499-550.
- [2] Lee, J. H. S., 2008, "The Detonation Phenomenon," Cambridge University Press.
- [3] Shepherd, J. E., 2009, "Structural Response of Piping to Internal Detonation," *Journal of Pressure Vessel Technology*, 131(3), pp. 031204.031201-031204.031213.
- [4] Harris, C. M., and Peirsol, A. G., 2002, *Harris' Shock and Vibration Handbook*, McGraw-Hill, NY.
- [5] McConnell, K. G., 1995, *Vibration Testing: Theory and Practice*, Wiley.
- [6] Paz, M., 1985, *Structural Dynamics Theory and Computation*, Van Nostrand Reinhold.
- [7] Antaki, G., 2003, *Piping and Pipeline Engineering*, Marcel Dekker, New York, NY.
- [8] Rao, K. R., 2002, *Companion Guide to the ASME Boiler and Pressure Vessel Code*, ASME Press.

- [9] Rodriguez, E., and Duffey, T., 2004, "Fracture-safe and fatigue design criteria for detonation-induced pressure loading in containment Vessels," Bulletin No. 494, Welding Research Council, New York, NY.
- [10] Duffey, T., Rodriguez, E., and Romero, C., 2002, "Design of pressure vessels for high strain rate loading," Bulletin No. 477, Welding Research Council, New York, NY.
- [11] Beltman, W. M., and Shepherd, J. E., 2002, "Linear elastic response of tubes to internal detonation loading," Journal of Sound and Vibration, 252(4), pp. 617-655.
- [12] Shepherd, J. E., Karnseky, J., Pintgen, F., and Krok, J. C., 2008, "Experimental measurements of strains and blast waves resulting from detonations in tubes," GALCIT Report FM2006.010, Pasadena, CA.
- [13] Shepherd, J. E., Teodorczyk, A., Knystautas, R., and Lee, J. H. S., "Shock Waves produced by Reflected Detonations," Proc. Progress in Astronautics and Aeronautics, AIAA, pp. 244-264.
- [14] Karnesky, J., Damazo, J., Shepherd, J. E., and Rusinek, A., "Plastic Response of Thin-Walled Tubes to Detonation," ASME.
- [15] Thomas, G. O., 2002, "The Response of Pipes and Supports to Internal Pressure Loads Generated by Gaseous Detonations," Journal of Pressure Vessel Technology, 124(1), pp. 66-73.
- [16] Shepherd, J. E., and Akbar, R., 2010, "Piping System Response to Detonations. ES1, TS1, and SS1 testing," GALCIT Report FM2009.001, Pasadena, CA.
- [17] Brown, S., Zeigler, J., and Shepherd, J. E., 2008, "Numerical Solution Methods for Shock and Detonation Jump Conditions," Technical Report No. FM2006.006, Graduate Aeronautical Laboratories - California Institute of Technology, Pasadena, CA.
- [18] Blevins, R. D., 1979, Formulas for Natural Frequency and Mode Shape, Kreiger Publishing Company, Malabar, FL.
- [19] Meyers, M. A., 1994, Dynamic Behavior of Materials, Wiley and Sons, New York, NY.
- [20] Rodabaugh, E. C., 1984, "Sources of uncertainty in the calculation of loads on supports of piping systems," No. NUREG/CR-3599, Oak Ridge National Laboratory, Oak Ridge, TN.
- [21] Shepherd, J. E., and Akbar, R., 2008, "Forces due to detonation propagation in a bend," GALCIT Report FM2008.002, Pasadena, CA.
- [22] Gordon, S., and McBride, B., 1994, "Compute Program for Calculation of Complex Chemical Equilibrium Compositions and Applications," Reference Publication No. RP-1311, NASA
- [23] Liang, Z., Curran, T., and Shepherd, J. E., 2008, "Structural response of piping components to detonation loading," GALCIT Report FM2006-008, Pasadena, CA.
- [24] Moody, F. J., 1990, Introduction to Unsteady Thermofluid Dynamics, J Wiley and Sons.
- [25] Olson, D. E., 2002, "Pipe Vibration Testing and Analysis " Companion Guide to the ASME Boiler and Pressure Vessel Code, K. R. Rao, ed., ASME Press.
- [26] Timoshenko, S. P., 1956, Strength of Materials - Part II Advanced Theory and Problems, Robert E. Krieger.

ⁱ This is the case for a 90-degree bend. For bends at other angles, the force will act along the bisector of the arc describing the bend and the magnitude will be reduced by $\sqrt{1 - \cos \theta}$ where θ is the bend angle.